Field-induced transition within the superconducting state of $CeRh_2As_2$

S. Khim, [1†*] J. F. Landaeta, [1†] J. Banda, [1] N. Bannor, [1] M. Brando, [1]

P. M. R. Brydon, [2] D. Hafner, [1] R. Küchler, [1] R. Cardoso–Gil, [1] U. Stockert, [1]

A. P. Mackenzie, [1,3] D. F. Agterberg, [4] C. Geibel, [1] and E. Hassinger [1,5*]

[1]Max Planck Institute for Chemical Physics of Solids, 01187 Dresden, Germany

[2]Department of Physics and MacDiarmid Institute for Advanced Materials and Nanotechnology,

University of Otago, P.O. Box 56, Dunedin 9054, New Zealand

[3]Scottish Universities Physics Alliance, School of Physics and Astronomy, University of St Andrews, St Andrews KY16 9SS, United Kingdom

[4]Department of Physics, University of Wisconsin-Milwaukee, Milwaukee, Wisconsin 53201, USA

[5]Technical University Munich, Physics department, 85748 Garching, Germany

[†]These authors contributed equally to the research.

[*]Correspondence should be addressed to elena.hassinger@cpfs.mpg.de and seunghyun.khim@cpfs.mpg.de

Materials with multiple superconducting phases are rare. Here, we report the discovery of two-phase unconventional superconductivity in $CeRh_2As_2$. Using thermodynamic probes, we establish that the superconducting critical field of its high-field phase is as high as 14 T, even though the transition temperature is only 0.26 K. Furthermore, a transition between two different superconducting phases is observed in a c-axis magnetic field. Local inversion-symmetry breaking at the Ce sites enables Rashba spin-orbit coupling alternating between the Ce sublayers. This introduces a layer degree of freedom to which the field-induced transition and high critical field seen in experiment is likely related.

The vast majority of unconventional superconductors have simple, single-component phase diagrams. This is surprising because the nature of superfluidity in ^{3}He (*1*) and the fact that degeneracies or near-degeneracies can be expected to result from many of the electronic mechanisms for unconventional superconductivity (*2*) suggest that a number of materials should feature temperature - magnetic field phase diagrams with transitions between different superconducting order parameters within the superconducting state. Until now, however, the only stoichiometric superconductor that has been well established to have such a phase diagram at ambient pressure is UPt_3 (*3-5*).

Here we report the discovery of this type of phase diagram in the heavy-fermion material $CeRh_2As_2$. Experimentally, we show that it has extremely high superconducting critical fields of up to 14 T in spite of a superconducting transition temperature T_c of only 0.26 K. Further, when the magnetic field is applied along the crystallographic c-axis, the superconducting state contains a well-defined internal phase transition at approximately 4 T that we identify using several thermodynamic probes. We also show that these observations result from physics different to that at play in UPt_3; the key superconducting properties of $CeRh_2As_2$ are likely a manifestation of local inversion symmetry breaking and consequent Rashba spin-orbit coupling in an overall inversion-symmetric crystal structure (*6- 13*), a situation for which multi-phase superconductivity has been considered in the theoretical literature (*13-15*), but not observed in a material so far. Combined with intriguing normal state physics that likely also results from the unusual crystalline environment of Ce, our observations suggest that $CeRh_2As_2$ will be a benchmark material in which to study the influence of spin-orbit coupling on electronic mechanisms for unconventional superconductivity.

Heavy-fermion superconductivity in $CeRh_2As_2$

$CeRh_2As_2$ crystallizes in the centrosymmetric tetragonal $CaBe_2Ge_2$-type structure (*16*) (Fig. 1A) in which Ce is alternatively stacked with two different Rh-As blocks along the c-axis; Rh(1) (As(1)) is tetrahedrally coordinated by As(2) (Rh(2)). There are two Ce atoms per unit cell. The Ce site lacks local inversion symmetry with the polar C_{4v} point group. The lattice inversion center lies in the middle of the line connecting the two Ce atoms. We believe this intriguing structure feature plays a central role in the physics of the superconducting state.

The high-temperature magnetization of single-crystalline $CeRh_2As_2$ shows paramagnetic Curie-Weiss behavior with an effective moment of 2.56 μ_B per Ce, corresponding to a Ce^{3+} valence state (Fig. 1B). In the whole temperature range, the ab-plane magnetization is larger than the c-axis one, by up to a factor of two at low temperature. The resistivity $\rho(T)$ depicted in Fig. 1C displays typical heavy-fermion behavior with increasing resistivity upon decreasing temperature owing to the Kondo effect. At temperatures below a characteristic local maximum at approximately 40 K, $\rho(T)$ decreases when the heavy quasi-particle bands are formed by hybridization of local 4f electrons with the conduction electrons. The large thermopower $S(T)$ is typical for a Kondo lattice system (Fig. 1D and (*17*)). Below 4 K the specific heat $C(T)/T$ in Fig. 1E (where the nuclear contribution has been removed (*17*)) increases towards low temperature following a power law with $C/T \propto T^{-0.6}$, suggesting non-Fermi liquid behavior and proximity to a quantum critical point (*18*). It reaches a large value of 1 J/mol-K^2 at

$T = 0.5$ K. The Kondo temperature in $CeRh_2As_2$ is between 20 K and 40 K, as estimated from the magnetic entropy $S_{mag}(T)$ shown in Fig. 1F (*17*). Interestingly, S_{mag} monotonically increases to reach the value $R \ln 4$ without a plateau at $R \ln 2$, where R is the ideal gas constant, suggesting that the two low-lying doublets of the crystal electric field (CEF) are very close in energy. The estimated separation of $\sim$ 30 K that is comparable with the Kondo energy could lead to a possible quasi-quartet ground state (*17, 19*). This is a rare example among the tetragonal Ce systems which usually exhibit a separation of $\gtrsim$ 100 K and again highlights the unusual local Ce environment in $CeRh_2As_2$.

Below 1 K, two anomalies appear in the specific heat as shown in Fig. 1E and G. A small hump is visible at $T_0 \approx 0.4$ K where the data depart from the power-law behavior extrapolated from high temperatures which is depicted by the dashed line. It hints at a phase transition to an ordered state. The large jump below 0.3 K results from the transition to a superconducting state involving the f electrons. An equal entropy analysis reveals $T_c = 0.26$ K and a height of the jump at T_c of $\Delta C/C|_{T_c} \approx 1$, similar to the Bardeen-Cooper-Schrieffer (BCS) value of 1.4. The residual Sommerfeld coefficient $\gamma = C/T$ for $T \to 0$ is possibly a sign of impurities. The diamagnetic drop of the ac-susceptibility confirms entry to the superconducting state (Fig. 1H) at a similar T_c for the transition midpoint but a slightly higher onset temperature; the first drop in resistivity takes place at 0.39 K (Fig. 1I). Although this is close to T_0 in zero field, the increase of T_0 with in-plane fields (see the specific heat data at 8 T and 12 T in Fig. 2A) shows that T_0 is not associated with superconductivity but likely signals some other kind of order. Its origin is yet to be determined, but the absence of an anomaly in the magnetic susceptibility at T_0 suggests that it might have Ce-4f multipolar or nematic character. We ascribe the higher T_c in the resistivity

and susceptibility to inhomogeneity in the material as known from other heavy-fermion systems (*20-22*). As a summary of these first results, $CeRh_2As_2$ is a heavy-fermion superconductor where the lowest CEF levels are separated by an energy of similar size as the Kondo temperature, both of the order of 30 K. Just before becoming superconducting at low temperature the system enters a state of unknown origin. For the remainder of this paper, we focus on the extraordinary superconducting properties as established experimentally using magnetic susceptibility and thermodynamic probes.

In Fig. 2 we show the temperature dependence of the specific heat C/T (panels A and B) and the magnetic ac-susceptibility χ'_{ac} (panels C and D) for different magnetic fields between 0 T and 14 T for $H \parallel ab$ (A and C) and $H \parallel c$ (B and D). T_c is defined via the equal entropy method in C/T and at the onset of the susceptibility transition (chosen arbitrarily by the temperature where χ'_{ac} has dropped to the value indicated by the dashed line). It shifts down with increasing field. In χ'_{ac} we observe a relatively strong shift of T_c in a field of 0.1 T that is absent in the specific heat, again a sign of non-bulk superconductivity (Fig. S7 in (*17*)). Increasing the field further reduces T_c more slowly. The superconducting transition is completely suppressed down to 0.05 K at magnetic fields of 14 T for $H \parallel c$ and 2 T for $H \parallel ab$. We note that, especially for $H \parallel c$, these are remarkably large critical fields for a superconductor with at T_c of only 0.26 K. For $H \parallel c$ the temperature sweeps (Fig. 2, B and D) imply a kink in the $T_c(H)$ curve where above 4 T, the decrease of T_c is slower than below this field.

Two superconducting phases

A pronounced kink in $T_c(H)$ is suggestive of the existence of two superconducting phases. Indeed, this is confirmed by field sweeps of the ac-susceptibility and two separate thermodynamic probes, magnetization and magnetostriction (Fig. 3, A-C). Remarkably, all three provide striking evidence of a phase transition. Below $T = 0.2$ K, pronounced kinks in all three observables are seen at a characteristic field, $H^\star = 3.9$ T, that is almost temperature independent as it increases from 3.8 T at 0.05 K to 4.0 T at 0.17 K. As shown in Fig. 3A and the inset of Fig. 3B, diamagnetic shielding and zero resistivity persist throughout the entire region of interest, further proving that this is a phase transition within the superconducting state. In contrast, field-dependent data for $H \parallel ab$ show no sign of such a phase transition (Fig. S7 in (*17*)).

Using the values of T_c, H_{c2} (defined in $\chi'_{ac}(H)$ at the onset in the same way as in the temperature sweeps) and $H^\star$ from our measurements, we show the superconducting phase diagrams of $CeRh_2As_2$ for out-of-plane and in-plane fields in Fig. 4, A and B, respectively. From these phase diagrams the superconducting critical field can be extrapolated to $H_{c2}(0) \approx 14$ T for $H \parallel c$ and 1.9 T for $H \parallel ab$. For $H \parallel c$ two superconducting states appear, labelled as SC1 and SC2, separated by a line that intersects the strong kink in the $H_{c2}(T)$ curve in a multi-critical point.

It is useful to estimate the upper critical fields with the Werthamer-Helfand-Hohenberg (WHH) formula $H_{orb} \approx 0.693\, T_c\, (-\frac{dH_{c2}}{dT})_{T_c}$ which only uses parameters near T_c where Pauli paramagnetic pair-breaking effects are parametrically suppressed (*23*). Using the large experimental slopes $(-\frac{dH_{c2}}{dT})_{T_c} = 97$ T/K for $H \parallel c$ and $(-\frac{dH_{c2}}{dT})_{T_c} = 45$ T/K for $H \parallel ab$, this yields $H_{orb} \approx 17$ T and $H_{orb} \approx 8$ T, respectively. Their anisotropy of a factor of ≈ 2 reflects

the anisotropy of the effective mass since $H_{orb} \propto m^{\star\,2}$ (*24*). The corresponding BCS coherence lengths $\xi = \sqrt{\Phi_0/2\pi H_{c2}(T=0)}$ are accordingly small, lying below 100 Å. The H_{orb} estimates suggest that the upper critical field of SC2 along the c-axis is not Pauli-paramagnetically suppressed. In contrast, we find that the superconducting state SC1 is strongly Pauli limited with Pauli critical fields that are enhanced compared to the Clogston-Chandrasekhar limit ($H_P \approx 0.5$ T) and 3 times larger for $H \parallel c$ than for $H \parallel ab$. This factor represents the scaling factor of the experimental critical field of SC1 for the two magnetic field directions.

The role of spin-orbit coupling

We begin with a summary of our key results on the superconducting properties of $CeRh_2As_2$. These are:

i) A large anisotropy in the critical fields, with a c-axis critical field (14 T) far exceeding the in-plane critical field (1.9 T). Indeed $\mu_0 H_{c2}/T_c$ for c-axis fields achieves the highest value so far observed in heavy-fermion superconductors.

ii) A superconducting state SC1 from which a second c-axis-field-induced superconducting phase, SC2, appears.

iii) The critical fields of SC1 are Pauli limited, in contrast to the critical field for SC2 and $H \parallel c$, which far exceeds the Pauli field.

iv) The c-axis Pauli field (5 T) for SC1 is signficantly larger than the in-plane Pauli field (1.9 T).

Our first finding, the large anisotropy in the critical fields and large c-axis critical field is

reminiscent of the non-centrosymmetric heavy-fermion superconductors $CeCoGe_3$, $CeRhSi_3$, and $CeIrSi_3$ (*25-29*) whose low crystal symmetry allows Rashba spin-orbit coupling (*29, 30*). Owing to the broken inversion symmetry in these materials, even-parity (spin-singlet) and odd-parity (spin-triplet) superconducting states are not distinct and are in general mixed. These mixed states generically reveal no Pauli paramagnetic suppression for fields along the c-axis whereas they do for in-plane fields (*29, 30*). However, these materials exhibit two important differences with respect to $CeRh_2As_2$: the first is that they do not exhibit multiple superconducting phases; the second is that inversion symmetry is preserved in $CeRh_2As_2$. Remarkably, these two differences lead to an explanation for our observation ii. Although $CeRh_2As_2$ is centrosymmetric, it is locally non-centrosymmetric, with an inversion symmetry linking two non-centrosymmetric Ce-square lattices, each of which has a Rashba interaction. A key feature of the centrosymmetric structure is that even-parity (spin-singlet) and odd-parity (spin-triplet) Cooper pairs are not mixed, so that a phase transition between even- and odd- parity condensates can occur. We argue below that this is the case in $CeRh_2As_2$. Indeed, a conceptually similar situation has been considered in models of bilayer materials, where the interplay between an intralayer Rashba interaction and interlayer hopping can lead to a c-axis field driven transition between two superconducting phases (*13- 15*), similar to that observed here. Below we show that the structure of $CeRh_2As_2$ allows this bilayer physics to appear in a crystalline setting.

To illustrate the relevance of spin-orbit coupling to determining the key physics of $CeRh_2As_2$ in spite of the presence of global inversion symmetry, we develop a model taking into account the unusual features of its structure. In particular, because Ce $4f$ electrons are key to the heavy quasi-particle bands that give rise to superconductivity, we consider Wannier

functions for these bands that are centered on the Ce sites. The Ce atoms sit at sites with a local C_{4v} symmetry, for which electronic states belong to CEF doublets of either Γ_6 or Γ_7 symmetry. A symmetry-based tight binding Hamiltonian, which takes the same form for either two Γ_6 or Γ_7 doublets, is

$$H_N = t_1[\cos(k_x) + \cos(k_y)] - \mu + \alpha_R \tau_z [\sin(k_x)\sigma_y - \sin(k_y)\sigma_x]$$

$$+t_{c,1}\tau_x \cos(\frac{k_z}{2})\cos(\frac{k_x}{2})\cos(\frac{k_y}{2}) + t_{c,2}\tau_y \sin(\frac{k_z}{2})\cos(\frac{k_x}{2})\cos(\frac{k_y}{2})$$

$$+\lambda\tau_z\sigma_z \sin k_z(\cos k_x - \cos k_y)\sin k_x \sin k_y. \quad (1)$$

Here, the σ_i Pauli matrices represent the two Kramer's spin-like degenerate states of the Γ_6 or Γ_7 doublets and the τ_i Pauli matrices represent the two Ce site degrees of freedom in each unit cell. Importantly, given that these two Ce site degrees of freedom are related by inversion symmetry, the τ_z matrix is odd under inversion symmetry (this follows because this matrix changes sign when the two Ce sites are interchanged). Inspection of Eq. 1 shows that a Rashba-like spin-orbit interaction, denoted by the constant α_R, is allowed by symmetry, with the odd inversion symmetry compensated by the τ_z operator. Equation 1 also reveals an additional Ising-like spin-orbit coupling term denoted by λ, with a $\tau_z\sigma_z$ dependence. This term will be much smaller than α_R because α_R originates from nearest neighbor $(a, 0, 0)$-type hoppings whereas λ requires much longer range $(a, 2a, c)$-type hoppings; for this reason we will set $\lambda = 0$ in the following. The two parameters $t_{c,i}$ correspond to c-axis $(a/2, a/2, c/2)$ hoppings between the two Ce sublattice sites.

Now we turn to the superconducting state. Density functional theory (DFT) reveals that the band structure for the conduction electrons is quasi two-dimensional, so it is natural to assume that the quasi-particle interactions that give rise to superconductivity originate in the

two-dimensional square Ce layers, which consist of only Ce sites from the same sublattice. So, in terms of τ_i operators, the Cooper pairs can have only a τ_0 or a τ_z dependence. Formally, τ_0 (τ_z) describes Cooper pair wavefunctions that have the same (opposite) sign on the two Ce sublattice sites. For simplicity, we will assume that each sublattice prefers a spin-singlet s-wave Cooper pair. This is not essential for the arguments presented below which rely on the τ_i structure of the Cooper pairs; the analysis also applies to a d-wave state such as those commonly found in tetragonal Ce materials. Below we explicitly consider the even parity gap function $\Delta_e = \Delta\tau_0$ and the odd parity gap function $\Delta_o = \Delta\tau_z$. We note that similar gap functions have been discussed in three-dimensional $Cu_xBi_2Se_3$ (*31*) and, remarkably, Δ_o-type gap functions were originally proposed by P. W. Anderson as the generic form of odd-parity superconductivity in heavy-fermion materials (*32*). These results indicate that Δ_e and Δ_o-type gap functions are stable solutions in general and not only in the quasi two-dimensional limit we consider here.

In (*17*) , we carry out a detailed analysis of Eq. 1 on the superconducting state by projecting onto a pseudospin basis. This analysis yields four generic results that apply to all superconducting states described in the previous paragraph. These are: i) The pairing interactions for Δ_e and Δ_o have the same sign (both are attractive); ii) Δ_e has a higher transition temperature than Δ_o in zero field; iii) Δ_e is Pauli suppressed by a c-axis field, whereas Δ_o is not (note the suppression of Δ_e by H_z is generically weaker than the usual paramagnetic suppression, i.e. the Pauli limit is enhanced). A c-axis field will therefore induce a first-order phase transition from Δ_e to Δ_o; iv) For in-plane fields both Δ_e and Δ_o are Pauli suppressed. These results naturally account for observations i) and ii). We then use a simplified model to fit the data, with the results shown in Fig. 4, C and D. These fits account for our

observations i-iv and suggest that the situation in $CeRh_2As_2$ is in close correspondence with that described in earlier theoretical work on a model for which, until now, there were no candidate materials (*14, 15*). Although the core results that we present here are experimental, and we do not claim that our simple model is a unique explanation for our findings, it is notable that the model succeeds in accounting for all our key observations.

As a final point, we look at the multi-critical point in the phase diagram for $H \parallel c$. In general, thermodynamic considerations forbid that three second-order transition lines meet at a multi-critical point (*33, 34*). However, the phase diagram as experimentally determined here for $H \parallel c$ is thermodynamically possible if one of the lines is of first order (*34*), and the model suggests that it is the line inside the superconducting state. Several experimental observations point to this scenario as well; an analysis of the slopes of the transition lines and their relation with the size of the specific heat jumps near the multicritical point is consistent with it (Fig. S8 and discussion in (*17*)). Furthermore, the dip in the magnetostriction at $H^\star$ corresponds to a step-like change of the sample length, and shows hysteresis of approximately 0.04 T (Fig. 3C and the inset). However, these experimental features are extremely small and not confirmed by any other probe, so the experimental evidence for the transition within the superconducting state being first order should not yet be regarded as conclusive.

At present we cannot exclude the possibility that the phase diagram including the normal state is more complicated. The putative ordered state below $T_0 \approx 0.4$ K also seems to be suppressed near $H \approx 4$ T (Fig. 2B) and the transition line might join the multi-critical point as a fourth transition line. Thermodynamically, this would allow the transition within the superconducting state to be second order and it would place further constraints on the slopes of

the lines and the ratios of the specific heat jumps. More generally, it is possible that the change of the superconducting state is influenced by a change in the normal state when the order below T_0 is suppressed. A more detailed study of the specific heat and the magnetocaloric effect would likely be able to resolve the issue.

It is intriguing to compare our findings with recent developments in UTe_2 (*35*, *36*). There, multi-phase superconductivity has been established in the $H-T$ phase diagram under the application of hydrostatic pressure (*37*) and a splitting of Tc has been reported at ambient pressure (*38*). A substantial body of theoretical work has been done on UTe_2 (*39-44*). The majority opinion is that the relevant phases are all triplet, and spin fluctuations are thought to be the main driver of the relevant physics. Spin fluctuations are a possible mechanism for superconductivity in $CeRh_2As_2$ as well. Typically these fluctuations stabilize either even or odd-parity states, but not both. However, in the unusual electronic environment of $CeRh_2As_2$, Rashba spin-orbit coupling allows both even and odd-parity states to be stabilized by the same underlying pairing interaction, opening up the possibility of an even to odd parity phase transition.

Outlook

Many open questions remain about the precise nature of the superconducting mechanism in $CeRh_2As_2$, including the possibility that the superconductivity in zero applied magnetic field condenses from a normal state that already includes unidentified order. Like the superconductivity, that 'hidden' order is probably rooted in the unusual Ce environment.

$CeRh_2As_2$ therefore highlights the importance of local symmetry breaking not just for superconductivity, but for metallic correlated electronic order as well.

References

1. A. J. Leggett, *Rev. Mod. Phys.* **47**, 331 (1975).

2. M. Sigrist, K. Ueda, *Rev. Mod. Phys.* **63**, 239 (1991).

3. R. A. Fisher, *et al.*, *Phys. Rev. Lett.* **62**, 1411 (1989).

4. S. Adenwalla, *et al.*, *Phys. Rev. Lett.* **65**, 2298 (1990).

5. R. Joynt, L. Taillefer, *Rev. Mod. Phys.* **74**, 235 (2002).

6. M. Shimozawa, S. K. Goh, T. Shibauchi, Y. Matsuda, *Rep. Progr. Phys.* **79**, 074503

(2016).

7. S. L. Wu, *et al.*, *Nat. Comm.* **8**, 1919 (2017).

8. K. Gotlieb, *et al.*, *Science* **362**, 1271 (2018).

9. H. Ishikawa, *et al.*, *Inorg. Chem.* **58**, 12888 (2019).

10. X. Zhang, Q. Liu, J.-W. Luo, A. J. Freeman, A. Zunger, *Nat. Phys.* **10**, 387 (2014).

11. L. Yuan, *et al.*, *Nat. Comm.* **10**, 906 (2019).

12. M. Fischer, F. Loder, and M. Sigrist, *Phys. Rev. B* **84**, 184533 (2011).

13. M. Sigrist, *et al.*, *J. Phys. Soc. Jap.* **83**, 061014 (2014).

14. T. Yoshida, M. Sigrist, Y. Yanase, *Phys. Rev. B* **86**, 134514 (2012).

15. D. Maruyama, M. Sigrist, Y. Yanase, *J. Phys. Soc. Jap.* **81**, 034702 (2012).

16. R. Madar, P. Chadouet, J. P. Senateur, S. Zemni, D. Tranqui, *J. Less-Common Met.* **133**, 303 (1987).

17. Materials and methods are available as supplementary materials.

18. A. Steppke, *et al.*, *Science* **339**, 933 (2013).

19. H. S. Jeevan, C. Geibel, Z. Hossain, *Phys. Rev. B* **73**, 020407(R) (2006).

20. E. Hassinger, *et al.*, *Phys. Rev. B* **77**, 115117(R) (2008).

21. M. D. Bachmann, *et al.*, *Science* **366**, 221 (2019).

22. J. F. Landaeta, *et al.*, *Phys. Rev. B* **97**, 104513 (2018).

23. N. R. Werthamer, E. Helfand, P. C. Hohenberg, *Phys. Rev.* **147**, 295 (1966).

24. J. P. Brison, *et al.*, *Physica C* **250**, 128 (1995).

25. M. -A. Méasson, *et al.*, *Physica C* **470**, S536-S538 (2010).

26. N. Kimura, *et al.*, *Phys. Rev. Lett.* **95**, 247004 (2005).

27. I. Sugitani, *et al.*, *J. Phys. Soc. Jap.* **75**, 043703 (2006).

28. N. Kimura, *et al.*, *Phys. Rev. Lett.* **98**, 197001 (2007).

29. E. Bauer, M. Sigrist, *Non-Centrosymmetric Superconductors : Introduction and Overview*, vol. 847 of *Lecture Notes in Physics* (Springer-Verlag, Berlin Heidelberg, 2012).

30. M. Smidman, M. B. Salamon, H. Q. Yuan, D. F. Agterberg, *Rep. Prog. Phys.* **80**, 036501 (2017).

31. L. Fu, E. Berg, *Phys. Rev. Lett.* **105**, 097001 (2010).

32. P. W. Anderson, *Phys. Rev. B* **32**, 499(R) (1985).

33. A. J. Leggett, *Prog. Theor. Phys.* **51**, 1275 (1974).

34. S. K. Yip, T. Li, P. Kumar, *Phys. Rev. B* **43**, 2742 (1991).

35. S. Ran, *et al.*, *Science* **365**, 684 (2019).

36. D. Aoki, K. Ishida, J. Flouquet, *J. Phys. Soc. Jap.* **88** 022001 (2019).

37. D. Aoki, *et al.*, *J. Phys. Soc. Jap.* **89**, 053705 (2020).

38. I. M. Hayes, *et al*., *Science* (2021); DOI: 10.1126/science.abb0272

39. K. Machida, *J. Phys. Soc. Jap.* **89**, 065001 (2020).

40. S. Sundar, *et al.*, *Phys. Rev. B* **100**, 140502 (2019).

41. Y. Xu, Y. Sheng, Y.-F. Yang, *Phys. Rev. Lett.* **123**, 217002 (2019).

42. J. Ishizuka, S. Sumita, A. Daido, Y. Yanase, *Phys. Rev. Lett.* **123**, 217001 (2019).

43. J. Ishizuka, Y. Yanase, *Phys. Rev. B* **103**, 094504 (2021).

44. T. Shishidou, *et al.*, *Phys. Rev. B* **103**, 104504 (2021).

45. S. Khim, *et al*., *Raw Data for "Field-induced transition within the superconducting state of $CeRh_2As_2$"*. Max Planck Society (2021); https://dx.doi.org/10.17617/3.72

46. H. Wilhelm, *et al.*, *Rev. Sci. Instrum.* **75**, 2700 (2004).

47. R. Küchler, T. Bauer, M. Brando, F. Steglich, *Rev. Sci. Instrum.* **83**, 095102 (2012).

48. T. Sakakibara, *et al.*, *Jpn. J. Appl. Phys.* **33**, 5067 (1994).

49. U. Köhler, *et al.*, *Phys. Rev. B* **77**, 104412 (2008).

50. F. Pobell, *Matter and Methods at Low Temperatures* (Springer-Verlag, 2007).

51. A. Steppke, *et al.*, *Phys. Status Solidi (b)* **247**, 737 (2010).

52. T. Hagino, Y. Seki, S. Takayanagi, N. Wada, S. Nagata, *Phys. Rev. B* **49**, 6822 (1994).

53. M. T. Hutchings, *Solid State Phys.* **16**, 227 (1964).

54. K. W. H. Stevens, *Proceedings of the Physical Society* **A65**, 209 (1952).

55. S.-K. Yip, *Phys. Rev. B* **87**, 104505 (2013).

56. L. Fu, *Phys. Rev. Lett.* **115**, 026401 (2015).

57. K. G. Wilson, *Reviews of Modern Physics* **47**, 733 (1976).

58. P. Fulde, R. Ferrell, *Phys. Rev.* **135**, A550 (1964).

59. A. I. Larkin, Y. N. Ovchinnikov, *Zh. Eksp. Teor. Fiz.* **47**, 1136 (1964).

60. G. M. Sheldrick, *SHELXL-97, Program for the Refinement of Crystal Structures* (University of Göttingen, Germany, 1997).

61. L. J. Farugia, *J. Appl. Cryst.* **45**, 849 (2012).

62. L. Akselrud, Y. Grin, *J. Appl. Crystallogr.* **47**, 803 (2014).

Acknowledgments

We strongly appreciated discussions with David Cavanagh, Onur Erten, Mark Fischer, Jun Sung Kim, David Möckli, Aline Ramirez, Burkhard Schmidt, Manfred Sigrist, Peter Thalmeier, Hans-Ulrich Desgranges, Helge Rosner, Kenji Ishida, Yoichi Yanase, Gertrud Zwicknagl, and Steffen Wirth. We thank Markus König, Ulrich Burkhardt, Monika Eckert, and Sylvia Kostmann for EDX measurements.

Funding: We acknowledge funding of the Physics of Quantum Materials department and the research group "Physics of Unconventional Metals and Superconductors (PUMAS)" by the Max Planck Society. C.G. and E.H. acknowledge support from the DFG through grant GE 602/4-1 Fermi-NESt. P.M.R.B. was supported by the Marsden Fund Council from Government funding,

managed by Royal Society Te Apārangi. R.K. is supported by the German Science Foundation (DFG) through Project. No. KU 3287/1-1. D.F.A. was supported by the US Department of Energy, Office of Basic Energy Sciences, Division of Materials Sciences and Engineering under Award DE-SC0021971. The research environment in Dresden benefits from the DFG Excellence Cluster ct.qmat.

Author contributions: S.K. and C.G. grew the single crystals. S.K., J.F.L., J. B., N.B., M.B., D.H., R.K., U.K., E.H. performed the measurements and data analysis. R.C.-G. conducted single-crystal diffraction measurements. P.M.R.B. and D.F.A. constructed the theoretical model. S.K., J.F.L., M.B., D.H., U.S., A.P.M., D.F.A., C.G., and E.H. interpreted the data. All authors were involved in designing the experiment and writing the manuscript.

Competing interests: The authors declare that they have no competing interests.

Data and materials availability: The data presented in this manuscript are avaiable online at the Open Research Data Repository of the Max Planck Society (*45*).

Supplementary materials

Materials and Methods

Supplementary Text

Figs. S1 to S8

Tables S1 and S2

Eqs. S1 to S17

References (*46-62*)

Figure 1: **Crystal structure and heavy-fermion superconductivity in $CeRh_2As_2$.** The magnetic field $\mu_0 H = 0$ unless indicated otherwise. (**A**) Crystal structure of $CeRh_2As_2$. (**B**) Inverse magnetic susceptibility $\chi(T)$ (after subtracting a temperature (T)-independent contribution χ_0) in $\mu_0 H = 1$ T applied in the ab-plane (blue points) and along the c-axis (red points). The dashed line denotes the linear slope for the effective moment of Ce^{3+}. (**C**) The resistivity $\rho(T)$ with the current in the ab-plane, normalised at 300 K. (**D**) The thermopower $S(T)$ with a temperature gradient in the ab-plane. (**E**) The specific heat $(C - C_n)/T(T)$. A nuclear contribution C_n was subtracted at low T (17). The dotted line presents the $LaRh_2As_2$ data used to subtract the phonon contribution. The dashed line represents the power-law T-dependence. (**F**) The Ce magnetic entropy $S_{mag}(T)$. (**G-I**) Experimental signatures at the superconducting transition T_c and at the transition T_0, see the text for details. (**G**) Specific heat $(C - C_n)/T(T)$ including the same dashed line as in (E) and transition temperatures as indicated. (**H**) Normalised ac-susceptibility χ'_{ac}. (**I**) The normalised electrical resistivity $\rho(T)$.

Figure 2: **Evolution of the superconducting transition with magnetic fields.** Temperature dependence of the specific heat C/T (**A**) and the real part of the ac-susceptibility χ'_{ac} (**C**), respectively, for $H \parallel ab$. (**B**) and (**D**) same for $H \parallel c$. The dashed line in (C) and (D) indicates the value of χ'_{ac} where the onset temperature T_c is defined.

Figure 3: **Phase transition inside the superconducting state for $H \parallel c$.** (**A**) Absolute value of

the magnetic susceptibility χ'_{ac} for different temperatures as indicated. Inset: zoom on the transition at $H^{\star}$. (**B**) Magnetization M at 0.1 K. Inset: Resistivity at 0.1 K. (**C**) Magnetostriction at 0.12 K. Inset: zoom on the transition at $H^{\star}$. The dashed line is a guide to the eye indicating the $H^{\star}$ transition at approximately 3.9 T.

Figure 4: **Superconducting phase diagrams for $CeRh_2As_2$** (**A**) for $H \parallel c$ and (**B**) $H \parallel ab$. Different symbols are from different experimental probes, as indicated in (A). (**C**) Fits to the upper critical fields for even (dotted line) and odd parity (solid line) states and a fit to the first order phase boundary between an even and odd-parity state (solid blue line). (**D**) Fit to the upper critical field for an even parity state. For details of the fitting procedure see (*17*).

Figure 1

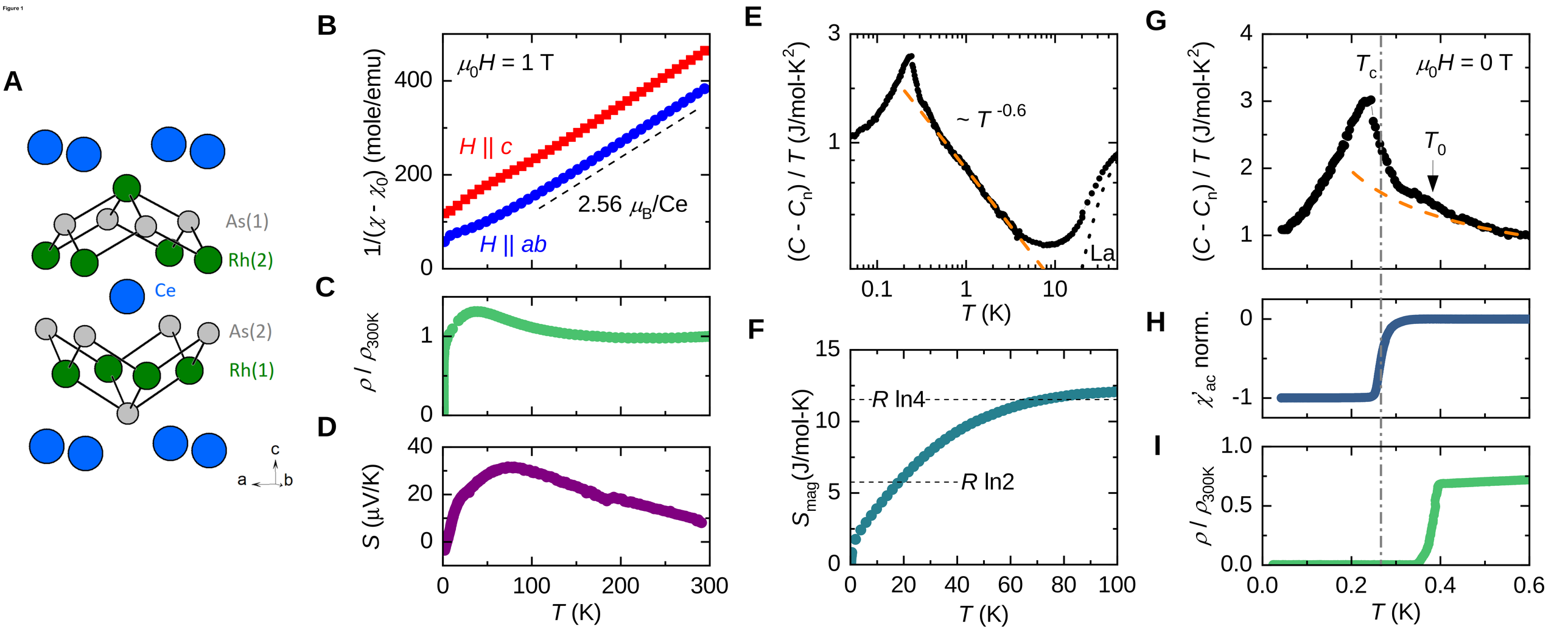
A
As(1)
Rh(2)
Ce
As(2)
Rh(1)
c
a
b
B
$\mu_0 H$ = 1 T
H || c
H || ab
2.56 μ_B/Ce
1/(χ - χ_0) (mole/emu)
C
ρ / ρ_{300K}
D
S (μV/K)
T (K)
E
(C - C$_n$) / T (J/mol-K^2)
~ T$^{-0.6}$
La
T (K)
F
S$_{mag}$(J/mol-K)
R ln4
R ln2
T (K)
G
T$_c$
$\mu_0 H$ = 0 T
T$_0$
(C - C$_n$) / T (J/mol-K^2)
H
χ'_{ac} norm.
I
ρ / ρ_{300K}
T (K)

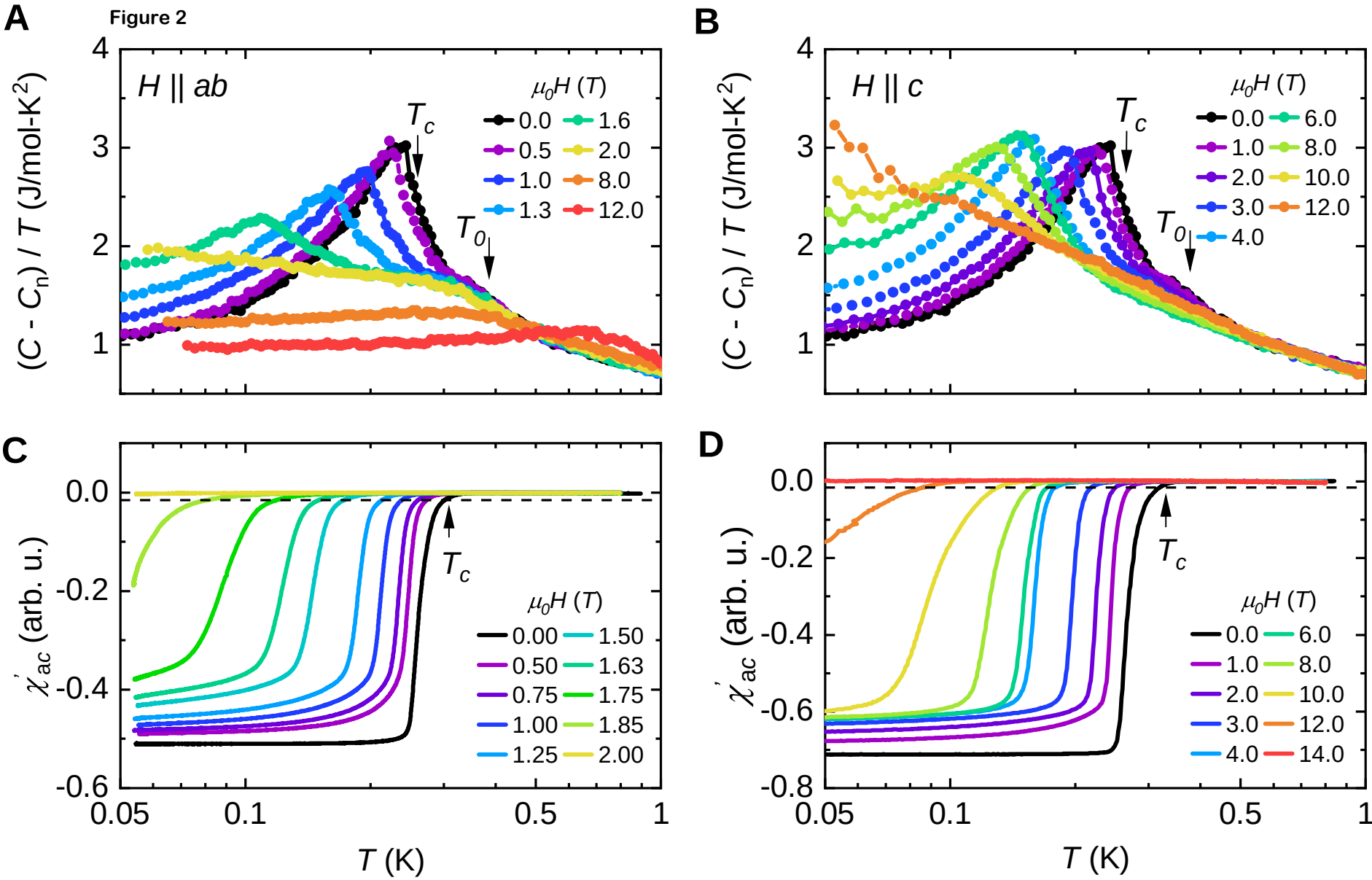
Figure 2
A
H || ab
T_c
T_0
μ_0H (T)
0.0
0.5
1.0
1.3
1.6
2.0
8.0
12.0
$(C - C_n) / T$ (J/mol-K^2)
B
H || c
T_c
T_0
μ_0H (T)
0.0
1.0
2.0
3.0
4.0
6.0
8.0
10.0
12.0
C
χ'_{ac} (arb. u.)
T_c
μ_0H (T)
0.00
0.50
0.75
1.00
1.25
1.50
1.63
1.75
1.85
2.00
T (K)
D
χ'_{ac} (arb. u.)
T_c
μ_0H (T)
0.0
1.0
2.0
3.0
4.0
6.0
8.0
10.0
12.0
14.0
T (K)

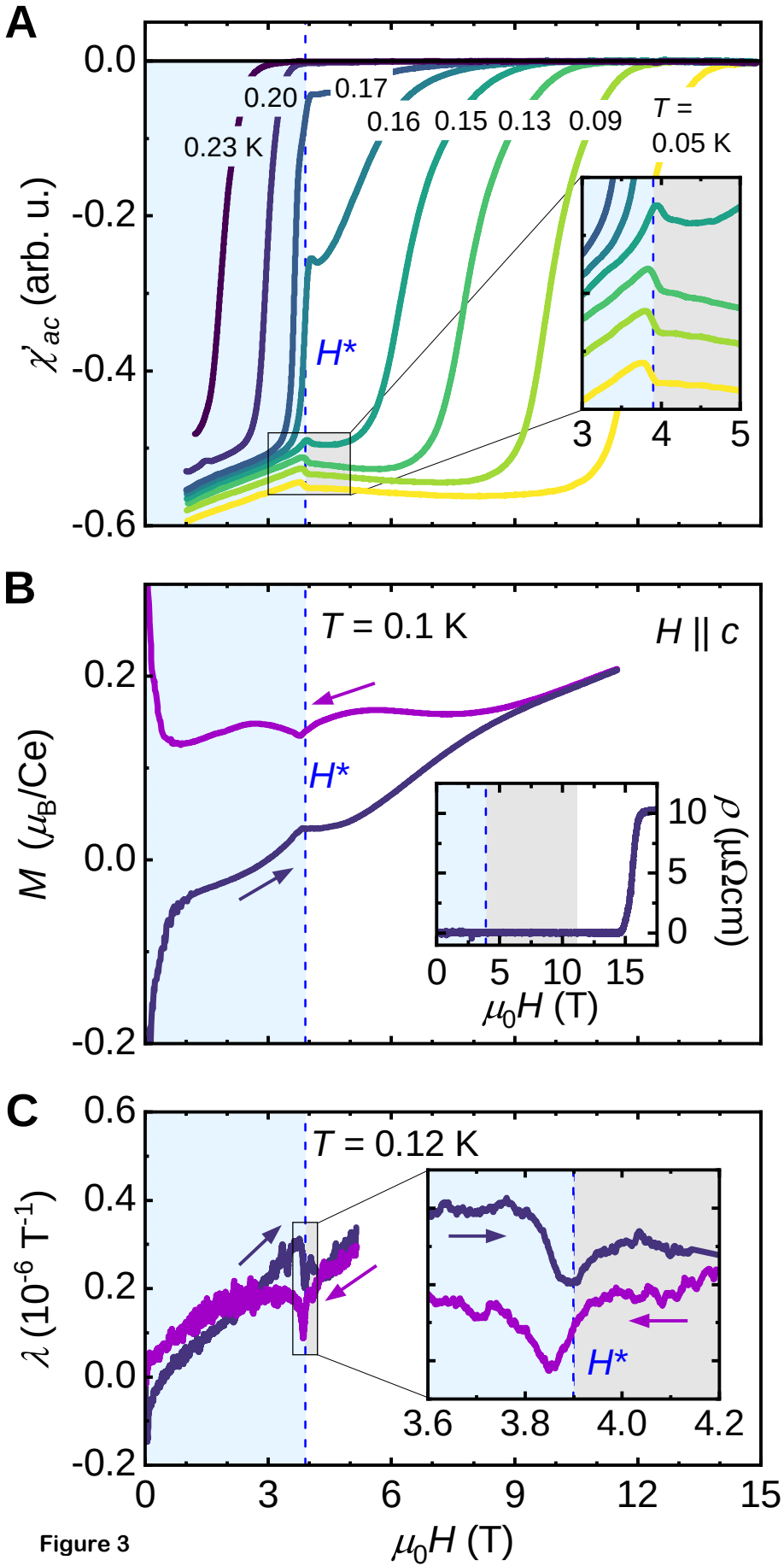
A
0.0
-0.2
-0.4
-0.6
χ'_{ac} (arb. u.)
0.23 K
0.20
0.17
0.16
0.15
0.13
0.09
T = 0.05 K
H*
3
4
5
B
T = 0.1 K
H || c
0.2
0.0
-0.2
M (μ_B/Ce)
H*
10
5
0
ρ ($\mu\Omega$cm)
0
5
10
15
$\mu_0 H$ (T)
C
T = 0.12 K
0.6
0.4
0.2
0.0
-0.2
λ (10^{-6} T^{-1})
H*
3.6
3.8
4.0
4.2
0
3
6
9
12
15
$\mu_0 H$ (T)

Figure 3

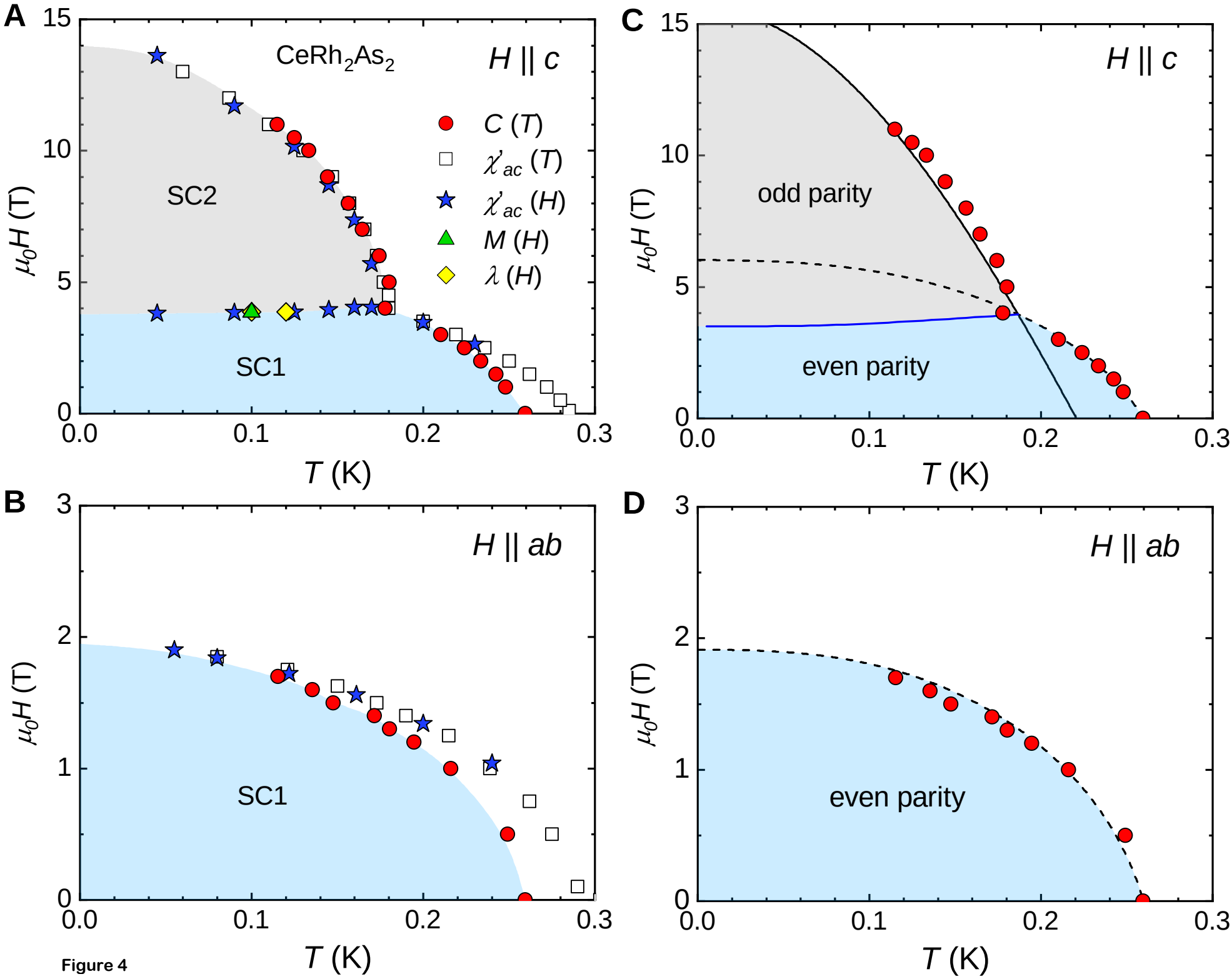
A
B
C
D
CeRh2As2
H || c
H || ab
C (T)
χ'ac (T)
χ'ac (H)
M (H)
λ (H)
SC2
SC1
odd parity
even parity
μ0H (T)
T (K)
0
5
10
15
0.0
0.1
0.2
0.3
1
2
3

Figure 4